Image analysis by moment invariants using a set of step-like basis functions

S. Dominguez *

CAR UPM-CSIC, Centre for Automation and Robotics, Spain

Keywords:
Moment invariants
Zernike moments
Image retrieval
Pattern recognition

A B S T R A C T

Moment invariants have been thoroughly studied and repeatedly proposed as one of the most powerful tools for 2D shape identification. In this paper a set of such descriptors is proposed, being the basis functions discontinuous in a finite number of points. The goal of using discontinuous functions is to avoid the Gibbs phenomenon, and therefore to yield a better approximation capability for discontinuous signals, as images. Moreover, the proposed set of moments allows the definition of rotation invariants, being this the other main design concern. Translation and scale invariance are achieved by means of standard image normalization. Tests are conducted to evaluate the behavior of these descriptors in noisy environments, where images are corrupted with Gaussian noise up to different SNR values. Results are compared to those obtained using Zernike moments, showing that the proposed descriptor has the same performance in image retrieval tasks in noisy environments, but demanding much less computational power for every stage in the query chain.

1. Introduction

Moment invariants have become a major topic in image description research from their initial proposal by Hu (1962). From then on, many attention has been paid to improve the theoretical basis of their definition and to generate new and better ways of building such descriptors (Reiss, 1991; Flusser and Suk, 2009). One of the main streams in this research has been to define moment invariants using orthonormal basis, given the links between them and Fourier decompositions postulated by Hilbert algebra; according this theoretical corpus, in addition to the advantages of using invariants, orthonormal basis offer optimal image description and reconstruction, in terms of computational effort (Rudin et al., 1991; Teague, 1980). In this way, many works have been devoted to explore the available orthonormal basis and their performance as image descriptors, setting comparative tests among them (Teh and Chin, 1988), or exploring their specific capabilities (Khotanzad and Hong, 1990). Given the description power that this kind of descriptors have shown for 2D images, some efforts have been devoted even to extend descriptions to 3D objects (Xu and Li, 2008). Recent efforts have been routed to mix the power of moment invariants with the analysis capabilities of waveletes, like (Chen et al., 2011).

In this paper, a set of orthonormal functions for moment invariants analysis is defined, being its main distinctive feature that they are discontinuous in a finite set of points, contrary to other well known moment sets, as Zernike or Legendre. This feature has been introduced in order to get a set that is well suited to analyse signals with discontinuities as well, like images have (Lee and Tarng, 1999), that originate undesired effects like Gibbs phenomenon when continuous functions are used to analyse them (Hewitt and Hewitt, 1979); it has been reported to generate visible artifacts in image reconstruction after filtering, as well (Bovik et al., 2009).

According to Hilbert Algebra, orthonormal basis have the property that descriptors obtained by projecting an image over each basis function contains exclusive information, i.e. it is not contained in any other descriptor of the series. This fact allows, in one hand, having the more compact representation in terms of descriptor series length, and on the other that images can be easily reconstructed just by combining their moment values, providing that the subspace spanned by the basis elements is dense (Rudin et al., 1991).

The goal of this work is, therefore, to generate a set of orthonormal functions that yields an image decomposition gathering the following properties:

- is well suited for analyzing 2D functions that may include step discontinuities, images in this case. It has been proved that discontinuous basis, like Haar, are well suited to analyze discontinuous signals.
- it allows the definition of rotation invariants, in order to generate the same descriptors for rotated instances of the same object.

In order to test the achievements of this work, results have been compared to those reached using Zernike moments; there are

* Tel.: +34 913363061; fax: +34 913363010.
E-mail address: sergio@etsii.upm.es

many works supporting the idea that Zernike moments are among the best suited sets of moments for image analysis (Teh and Chin, 1988; Chen et al., 2011).

2. Derivation of the basis functions

The general definition of moments is the following: given an image $I(x,y)$, its moment M_{nm} is computed as (Flusser and Suk, 2009):

$$M_{nm}(f) = \int_{x_0}^{x_f}\int_{y_0}^{y_f} p_{nm}(x,y)I(x,y)dx\,dy \tag{1}$$

where $p_{nm}(x,y)$ is a function which belongs to the moment basis, having orders n for the x component and m for the y, and $[x_0,x_f]$ and $[y_0,y_f]$ are the limits of the region where both the image $I(x,y)$ and $p_{nm}(x,y)$ are defined.

Note that according to Hilbert Algebra, Eq. (1) can be interpreted as the inner product between both functions, $\langle p_{nm}(x,y), I(x,y)\rangle$. This fact allows the introduction of the concept of orthonormality between each pair of functions belonging to the proposed basis.

In this work, the space to be analyzed is the 2D image domain, with the particularity that it is expressed in polar coordinates and restricted to the unit circle, instead the common cartesian coordinates; this representation has been used before, e.g. for Zernike moments based image analysis. Therefore, any image, $I(\rho,\theta)$, is defined as:

$$I(\rho,\theta):\Omega\mapsto[0,1],\quad \Omega=\{(\rho,\theta)\in\mathbb{R}^2:\ 0\leqslant\rho\leqslant 1,\ 0\leqslant\theta<2\pi\} \tag{2}$$

Given this workspace the proposed structure for the family of functions that build up the moments basis must depend upon parameters (ρ,θ), i.e. radial and an angular components. The radial component of each basis function, which will be named $\Pi_n(\rho)$ for its nth order, is built up by concatenating step-like functions, similar to Haar's, which commutes between -1 and 1, but removing the restriction that forces lower and upper steps to be of the same size. This radial analysis must be combined with an angular component, which in this case has been selected to be the Fourier basis, $e^{im\theta}$ for its mth order: this choice is due to the fact that it allows an easy generation of rotation invariants based on moment values, due to the following property (Flusser, 2000). Given a rotated version of an image, $I'(\rho,\theta)=I(\rho,\theta+\alpha)$, their nm moment are related by $\Phi'_{nm}=\Phi_{nm}e^{-im\alpha}$, so it can be easily stated that $\|\Phi_{nm}\|$, i.e. the magnitude of the complex value of nm moment, is a rotation invariant. Therefore, the generic formulation for one function of the proposed base is:

$$\varphi_{nm}(\rho,\theta)=\Pi_n(\rho)e^{im\theta},\quad \{n,m\}\in\mathbb{N} \tag{3}$$

being

$$\Pi_n(\rho)=u_0(\rho)+\sum_{i=1}^{n}(-1)^i\,2\,u_0(\rho-\rho_{ni}),\quad \rho\in[0,1],\quad \forall i,\rho_{ni}\in(0,1) \tag{4}$$

where $u_0(\rho-\alpha)$ represents a unit step triggered at $\rho=\alpha$.

Gathering all these conditions, the definition of the proposed set of moments turns to be:

$$\Phi_{nm}=\langle I(\rho,\theta),\varphi_{nm}(\rho,\theta)\rangle=\frac{1}{\pi}\int_0^{2\pi}\int_0^1 I(\rho,\theta)\varphi^*_{nm}(\rho,\theta)\,\rho\,d\rho\,d\theta \tag{5}$$

where * stands for the complex conjugate operator. Note that Eq. (5) corresponds to the transformation of Eq. (1) to polar coordinates.

Now, in order to follow the derivation that will be explained hereafter, the following notation is introduced: the radial component of the base functions, $\Pi_n(\rho)$, will be represented as the set of zero crossing points (ZCP), adding as well the beginning and the end of the interval for convenience: $\rho_{n0}=0,\ \rho_{nn+1}=1$. Therefore, from now on it will be written:

$$\Pi_n(\rho)\equiv\{\rho_n\}=\{0,\rho_{n1},\rho_{n2},\ldots,\rho_{nn},1\},\quad \forall i=1,\ldots,n,\ \rho_{ni}\in(0,1) \tag{6}$$

Given these definitions for the set of functions $\varphi_{nm}(\rho,\theta)$, the next step is to force the orthonormality condition among all of them. Let $\varphi_{nm}(\rho,\theta)$ and $\varphi_{kl}(\rho,\theta)$ be two functions belonging to the proposed base. Then their scalar product must be:

$$\langle\varphi_{nm}(\rho,\theta),\varphi_{kl}(\rho,\theta)\rangle=\frac{1}{\pi}\int_0^{2\pi}\int_0^1\varphi_{nm}(\rho,\theta)\varphi^*_{kl}(\rho,\theta)\rho\,d\rho\,d\theta=\delta_{nk}\delta_{nl} \tag{7}$$

where

$$\delta_{uv}=\delta(u-v)=\begin{cases}1 & u=v\\ 0 & \text{otherwise}\end{cases} \tag{8}$$

Developing each basis function into its constituent parts, as described in Eq. (3), Eq. (7) becomes:

$$\langle\varphi_{nm}(\rho,\theta),\varphi_{kl}(\rho,\theta)\rangle=\frac{1}{\pi}\int_0^{2\pi}\int_0^1\Pi_n(\rho)e^{im\theta}\Pi_k(\rho)e^{-il\theta}\rho\,d\rho\,d\theta \tag{9}$$

Since terms depending on ρ and on θ are decoupled, i.e. no term of Eq. (9) depends upon both parameters, it can be written as:

$$\langle\varphi_{nm}(\rho,\theta),\varphi_{kl}(\rho,\theta)\rangle=\frac{1}{\pi}\int_0^1\Pi_n(\rho)\Pi_k(\rho)\left[\int_0^{2\pi}e^{im\theta}e^{\ il\theta}d\theta\right]\rho\,d\rho \tag{10}$$

as can be easily seen, the term into brackets is the scalar product of two elements of the Fourier base, which are known to be orthonormal, and therefore its clear that:

$$\int_0^{2\pi}e^{im\theta}e^{-il\theta}d\theta=2\pi\,\delta_{ml} \tag{11}$$

Then, entering with Eq. (11) in Eq. (10), the scalar product turns into:

$$\langle\varphi_{nm}(\rho,\theta),\varphi_{kl}(\rho,\theta)\rangle=2\delta_{ml}\int_0^1\Pi_n(\rho)\Pi_k(\rho)\rho\,d\rho \tag{12}$$

Therefore, and recalling the condition expressed in Eq. (7), the design of the orthonormal basis is reduced to the design of a unidimensional orthonormal basis using the functions proposed in Eq. (4) for describing the variation along ρ dimension, namely $\Pi_n(\rho)$. Then, it must be ensured that, from Eq. (12):

$$2\int_0^1\Pi_n(\rho)\Pi_k(\rho)\rho\,d\rho=\delta_{nk} \tag{13}$$

The case where $n=k$, which should equals Eq. (13) to 1, is trivial since $\Pi_n^2(\rho)=1,\ \forall\rho\in[0,1]$. Then, Eq. (13) must vanish $\forall n\neq k$.

First of all, the product of $\Pi_n(\rho)$ and $\Pi_k(\rho)$ must be computed. In order to obtain this result let's use the notation introduced in Eq. (6) to define:

$$\Pi_n(\rho)\Pi_k(\rho)\equiv\{\rho_n\}\cup\{\rho_k\}=\{\rho_{nk}\} \tag{14}$$

being $\{\rho_{nk}\}$ and ordered set such that:

$$\{\rho_{nk}\}=\{\rho_{nki}\in[0,1],\quad \forall i=1,\ldots,n+k,\ \rho_{nk,i}\in\{\rho_n\}\cup\{\rho_k\}:\rho_{nki}\geqslant\rho_{nk(i-1)},\ \rho_{nk0}=0,\ \rho_{nkn+k+1}=1\} \tag{15}$$

Using this notation it's easy to compute the integral described in Eq. (13), knowing that each element in $\{\rho_{nk}\}$ correspond to a ZCP of the product $\Pi_n(\rho)\Pi_k(\rho)$, starting with:

$$\Pi_n(\rho)\Pi_k(\rho)=1,\quad \forall\rho\in[0,\rho_{nk1}] \tag{16}$$

Then, back to Eq. (13) for the case $n\neq k$ and using the list in Eq. (15), it can be written:

$$2\int_0^1 \Pi_n(\rho)\Pi_k(\rho)\,\rho\,d\rho = 2\left[\sum_{k=0}^{k\leqslant\frac{m+l}{2}}\int_{\rho_{nk\,2i}}^{\rho_{nk\,2i+1}}\rho\,d\rho \quad - \sum_{k=1}^{k\leqslant\frac{m+l+1}{2}}\int_{\rho_{nk\,2i-1}}^{\rho_{nk\,2i}}\rho\,d\rho\right] = 0 \tag{17}$$

with each integral resulting in the difference of its squared limits:

$$2\int_0^1 \Pi_n(\rho)\Pi_k(\rho)\,\rho\,d\rho = \sum_{k=0}^{k\leqslant\frac{m+l}{2}}\left(\rho_{nk\,2i+1}^2 - \rho_{nk\,2i}^2\right) - \sum_{k=1}^{k\leqslant\frac{m+l+1}{2}}\left(\rho_{nk\,2i}^2 - \rho_{nk\,2i-1}^2\right) = 0 \tag{18}$$

Making use of Eq. (18) it is possible to build the set of equations which allows the derivation of the elements in $\{\rho_n\}$ and $\{\rho_k\}$. For this sake, it is necessary to define $\Pi_0(\rho)$ in advance, because it will be used to initialize the set of equations. Its definition is set as:

$$\Pi_0(\rho) = 1, \quad \forall\rho \in [0,1] \tag{19}$$

which corresponds to the definition of the zeroth order moment for other widely used families of moments, like Zernike or Legendre.

Departing from $\Pi_0(\rho)$, and forcing the condition expressed in Eq. (18) for the successive functions in the base, the following system of equations is derived, where the symbol $\perp$ denotes the orthogonality condition:

$$\begin{aligned}
&\Pi_0(\rho)\perp\Pi_1(\rho): \ \rho_{11}^2 = 1-\rho_{11}^2\\
&\Pi_0(\rho)\perp\Pi_2(\rho): \ \rho_{21}^2+(1-\rho_{22}^2) = \rho_{22}^2-\rho_{21}^2\\
&\Pi_1(\rho)\perp\Pi_2(\rho): \ \rho_{21}^2+(\rho_{22}^2-\rho_{11}^2) = (\rho_{11}^2-\rho_{21}^2)+(1-\rho_{12}^2)\\
&\Pi_3(\rho)\perp\Pi_0(\rho): \ \rho_{31}^2+(\rho_{33}^2-\rho_{32}^2) = (\rho_{32}^2-\rho_{31}^2)+(1-\rho_{33}^2)\\
&\Pi_3(\rho)\perp\Pi_1(\rho): \ \rho_{31}^2+(\rho_{11}^2-\rho_{32}^2)+(1-\rho_{33}^2)\\
&\qquad\qquad = (\rho_{32}^2-\rho_{31}^2)+(\rho_{33}^2-\rho_{11}^2)\\
&\Pi_3(\rho)\perp\Pi_2(\rho): \ \rho_{31}^2-(\rho_{33}^2-\rho_{21}^2)+(\rho_{33}^2-\rho_{22}^2)\\
&\qquad\qquad = (\rho_{21}^2-\rho_{31}^2)+(\rho_{22}^2-\rho_{32}^2)+(1-\rho_{33}^2)\\
&\ldots
\end{aligned} \tag{20}$$

Therefore, in order to calculate the set $\{\rho_n\}$ which defines $\Pi_n(\rho)$ a system of $\frac{n(n+1)}{2}$ equations with the same number of unknowns, namely the elements of $\{\rho_n\},\{\rho_{n-1}\},\ldots,\{\rho_1\}$, is generated.

It is worth to mention that it's possible that some mistake could be made in hypothesizing the relative position of elements of $\{\rho_n\}$ and $\{\rho_k\}$ during the process of intermingling them to build $\{\rho_{nk}\}$, but given the fact that the set of equations described in (20) can be solved progressively, from lower to upper orders, at the time of computing the position of the elements of one set, all the lower order sets are known, and since the solution for the equations is unique, the resulting set is always properly placed and ordered.

The results of solving the system of equations in (20) are shown in Fig. 1.

Note that this set of functions can straightforwardly be recognized as a warped version of the ordered Walsh function series, being the most notorious difference with respect to them that the ZCP distribution in the proposed set is unevenly distributed in the $[0,1]$ interval (Rao et al., 1983). After the derivation of this set of functions can be stated that they should be used to provide orthogonality in the ρ coordinate of a polar system, whilst the original Walsh functions should be used in the cartesian case.

3. Noise sensitivity

In real world applications images are seldom completely clean, having arbitrary amounts of noise. In this section, the proposed family of invariants is tested against images corrupted with different amounts of additive Gaussian noise, in order to check their ability to preserve image information from noise, following the experiment described in Teh and Chin (1988). For the sake of providing a baseline, results are compared to those obtained using Zernike moments under the same conditions.

Zernike moments are defined departing from Zernike polynomials:

$$R_{nm}(\rho) = \sum_{s=0}^{\frac{n-|m|}{2}}(-1)^s\frac{(n-s)!}{s!\left(\frac{n+|m|}{2}-s\right)!\left(\frac{n-|m|}{2}-s\right)!}\rho^{n-2s} \tag{21}$$

$$R(\rho) = \{R_{nm}(\rho)| \quad n=0,1,\ldots,\infty,\ |m|\leqslant n,\ n-|m| \text{ even}\}$$

and, from this definition, the Zernike moment of order nm of an image $I(\rho,\theta)$ is:

$$A_{nm} = \frac{n+1}{\pi}\int_0^{2\pi}\int_0^1 [V_{nm}(\rho,\theta)]^* I(\rho,\theta)\,\rho\,d\rho\,d\theta \tag{22}$$

where $V(\rho,\theta)$ is defined as:

$$V_{nm}(\rho,\theta) = R_{nm}(\rho)e^{im\theta} \tag{23}$$

Only the magnitude of its complex value $\|A_{nm}\|$, which is rotation invariant (Teague, 1980), will be used as a descriptor.

For this experiment, a set of one hundred images has been randomly extracted from our test database, which contains more than 30.000 binary, 128×128 normalized images; the normalization process ensures translation and scale invariance[1] (Khotanzad and Hong, 1990). A few samples of the images contained in this database can be seen in Fig. 2. For each of these images, four corrupted copies have been generated, adding Gaussian noise in order to create four noisy instances corresponding to $\text{SNR}_{in} = \{4,2,1,0.5\}$, being:

$$\text{SNR}_{in} = \frac{\sum_{\forall\{\rho,\theta\}}\left[I(\rho,\theta)-\bar{I}(\rho,\theta)\right]^2}{\sum_{\forall\{\rho,\theta\}}\left[n(\rho,\theta)-\bar{n}(\rho,\theta)\right]^2} \tag{24}$$

where $n(\rho,\theta)$ is the additive noise, and $\bar{I}$, $\bar{n}$ stand for the respective means of image and noise values (Chen et al., 2011). Note that by the addition of Gaussian noise to a binary image, a gray level instance is generated.

The moment transformation of each set of four images have been computed, using both families of moments; in both cases, only their norms are kept, $\|A_{nm}\|$, $\|\Phi_{nm}\|$. To evaluate the quality of the transformation after the addition of noise, the SNR_{nm} of each order of moments have been calculated, using:

- for Zernike moments, $\|A_{nm}\|$, being $m=0$ for n even and $m=1$ for n odd.
- for the proposed set, $\|\Phi_{nm}\|$, being $m=0$ for all values of n.

In this case, the SNR_{nm} of the moment set is defined as:

$$\text{SNR}_{nm} = \frac{\sum_{i=1}^{100}\left[\phi_{nm}^i - \bar{\phi}_{nm}\right]^2}{\sum_{i=1}^{100}\left[\kappa_{nm}^i - \bar{\kappa}_{nm}\right]^2} \tag{25}$$

where ϕ_{nm}^i stands for the moment ($\|A_{nm}\|$ or $\|\Phi_{nm}\|$) of the ith image, and κ_{nm}^i, stands for the moment ($\|A_{nm}\|$ or $\|\Phi_{nm}\|$) of the noise added to the ith image (Teh and Chin, 1988).

Results of this experiment are shown in Fig. 3. They have been generated extending the Zernike order up to 17th (dashed lines) and the proposed set up to 16th order (continuous lines). Representative numeric values are gathered in Table 1.

[1] Image database is available by sending a request by e-mail to the author.

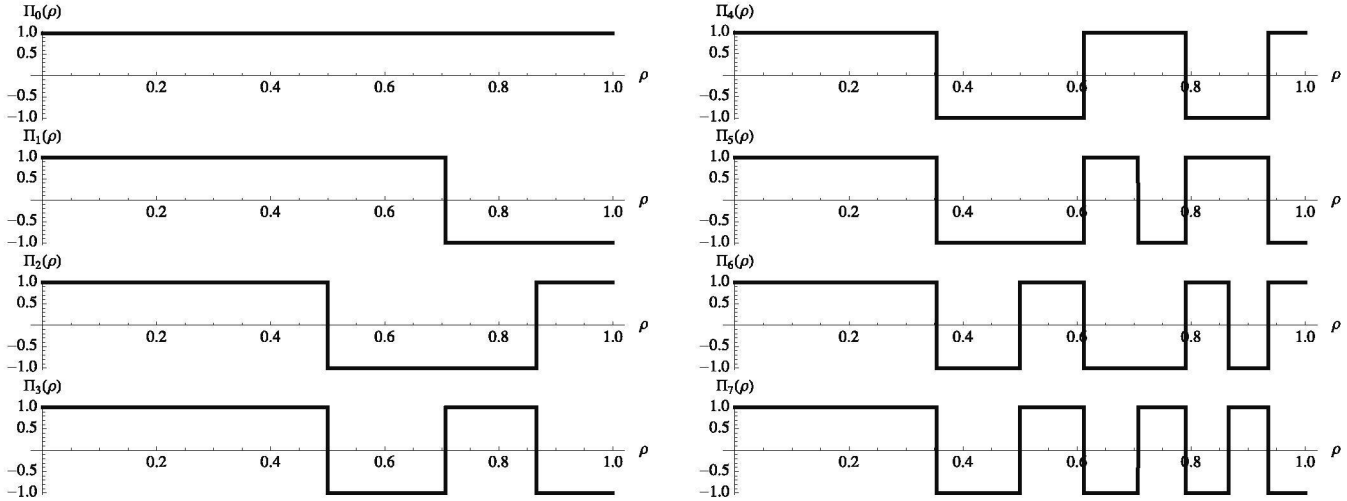

Fig. 1. Radial components of $\varphi_{nm}(\rho,\theta)$, i.e. $\Pi_n(\rho)$, up to seventh order.

Fig. 2. Examples of images contained in the database.

It can be observed that the slope of SNR_{nm} for the set $\|\Phi_{nm}\|$ in the presence of noise is slightly faster than for $\|A_{nm}\|$. It can be thereafter concluded that the analysis of images using $\|\Phi_{nm}\|$ cannot be extended to very high orders, because it could be possible to represent signal and noise with practically the same strength in a descriptor. This restriction will be applied in the following sections.

4. Results in image retrieval

The proposed family of invariants has been used as image descriptor in two image retrieval tasks in order to test it. Given the results shown in Section 3, their order has been kept very low, using the ranks $m = 0,\ldots,6,\ n = 0,\ldots,7$, which sum up a total of 56 descriptors per image. Zernike moments have been extracted up to 17th order, that according with (Teh and Chin, 1988 and Mukundan, 2004) represents a good tradeoff between quality of the representation and noise sensibility, giving a total of 90 descriptors per image. This means that the length of the description is roughly a 40% shorter using the proposed family of invariants. This would represent a very desirable reduction both in computing and storage in a real world application, but for this sake, the performance of this description should be as good as Zernike moments'.

The first retrieval experiment consisted of a set of 100 queries launched against our binary test database. The second has consisted of the same number of queries launched against a graylevel copy of CalTech 101 (Fei-Fei et al., 2004), which contains roughly 9.500 images categorized in 101 classes. The performance evaluation for each query has been carried out by comparing the retrieval precision, defined as:

$$\text{precision} = \frac{\text{images correctly retrieved}}{\text{number of retrieved images}} \tag{26}$$

Its complementary measure, recall, has not been available since labeling the complete binary database for each of the 100 queries results in an overwhelming task (it would be necessary to evaluate more than 3 million similarities).

In both cases the retrieved set size has been kept in 25 elements per query; every query has been resolved using both descriptors, $\|A_{nm}\|$ and $\|\Phi_{nm}\|$. Average precision has been computed for each retrieval set size ranging from 1 to 25. Results are depicted in Fig. 4.

As can be seen in Fig. 4, both sets of invariants yield almost the same performance in terms of their precision in an image retrieval task. This fact confirms that the proposed set is as good as Zernike moments for retrieval. Nevertheless, the proposed set of descriptors is a 40% shorter than the set of Zernike moments used for achieving the same result. This reduction carries out great benefits for a retrieval system, since it will reduce computational needs in every related task, in terms of:

- Storage requirements: the size of the database will be reduced in a 40%, reducing in the same proportion the storage needs.
- Computation time: since the computational cost of a single descriptor is the same in both cases, the reduction in size will be straightforwardly mirrored by the same reduction in computation time for the descriptor set.
- Indexing system: multidimensional indexing gets more complex as the size of the descriptor increases; the noticeable reduction in the descriptor set will therefore reduce the complexity of the indexing system, and increase consequently the overall performance of the search engine.

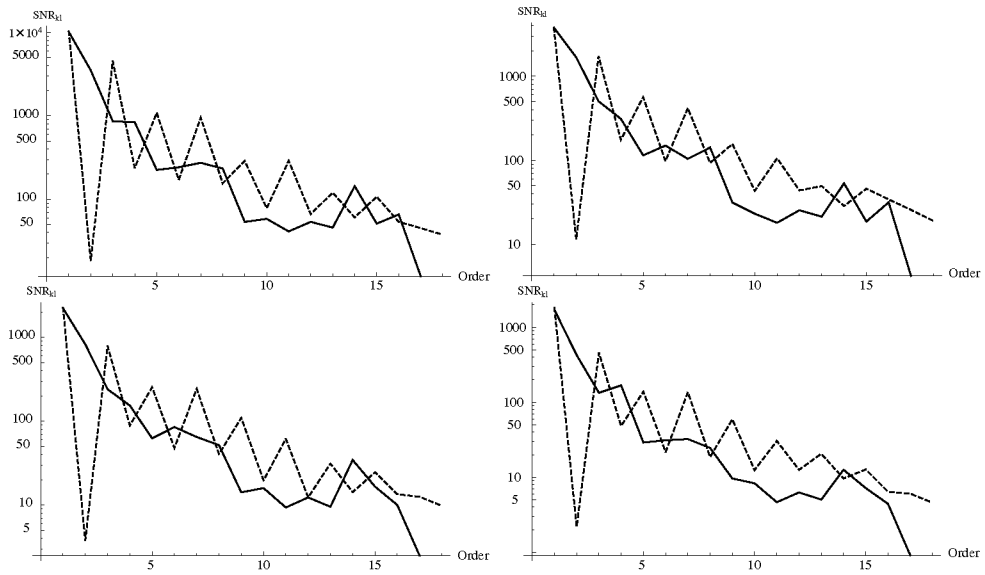

Fig. 3. SNR_{nm} of the invariants set against invariants order. In continuous line $\|\Phi_{nm}\|$; dashed, $\|A_{nm}\|$. Up down, left to right: $\mathrm{SNR}_{in} = 4$, $\mathrm{SNR}_{in} = 2$, $\mathrm{SNR}_{in} = 1$, $\mathrm{SNR}_{in} = 0.5$.

Table 1
Summary of results: SNR_{nm} stands for the SNR of each moment set at order n.

SNR_{in}	Set	SNR_{3m}	SNR_{6m}	SNR_{9m}	SNR_{12m}	SNR_{15m}
0.5	Zernike	48.21	136.16	12.44	20.61	6.41
	Proposed	168.09	32.33	8.30	5.03	4.42
1.0	Zernike	89.14	243.54	19.66	31.13	13.46
	Proposed	153.77	64.84	15.93	9.55	10.02
2.0	Zernike	174.291	416.76	43.28	49.23	34.20
	Proposed	310.89	103.89	23.10	21.30	31.55
4.0	Zernike	237.26	955.63	78.33	120.44	53.81
	Proposed	838.65	273.81	58.32	45.81	65.84

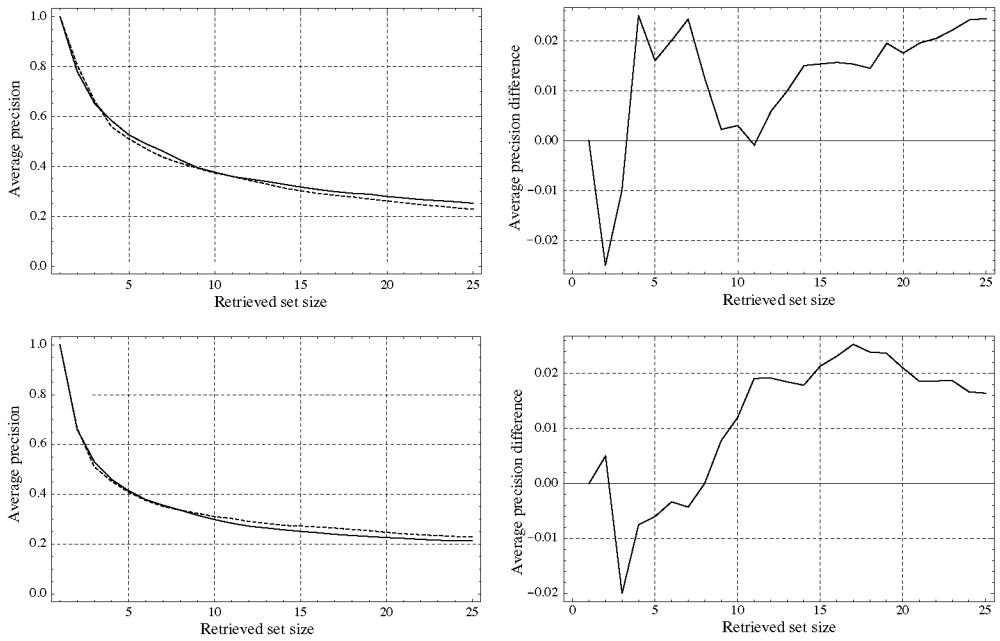

Fig. 4. Up: Results on binary images. Down: Results on graylevel images. Left: Comparison between average precision using $\|A_{nm}\|$ (dashed line) and $\|\Phi_{nm}\|$ (continuous line) for different retrieved set sizes. Right: Difference between them.

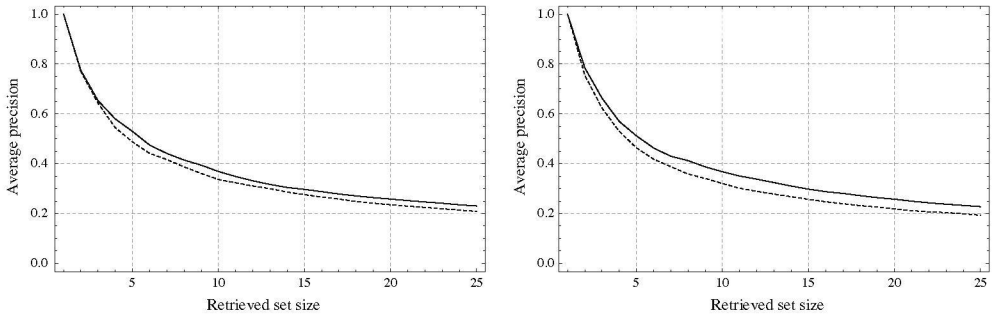

Fig. 5. Comparison between average precision using Zernike moments (dashed line) and the proposed family of moments (continuous line) for different retrieved set sizes: right, $SNR_{in} = 1$; left, $SNR_{in} = 0.5$.

Table 2
Summary of results: P_i stands for the average precision for a retrieval set containing i elements.

SNR_{in}	Set	# Moments	P_5	P_{10}	P_{15}	P_{20}	P_{25}
Noise free (binary)	Zernike	90	0.510	0.373	0.301	0.262	0.227
	Proposed	56	0.526	0.376	0.317	0.279	0.252
Noise free (graylevel)	Zernike	90	0.414	0.298	0.250	0.226	0.212
	Proposed	56	0.408	0.310	0.272	0.247	0.229
1.0	Zernike	90	0.488	0.337	0.276	0.235	0.209
	Proposed	56	0.520	0.369	0.297	0.259	0.231
0.5	Zernike	90	0.464	0.321	0.257	0.219	0.194
	Proposed	56	0.512	0.368	0.298	0.258	0.228

- Comparison time: Ranking algorithms need to compute a metric function over two descriptor sets in order to assess whether the two corresponding images are similar or not. This task will benefit from this size reduction as well.

An additional experiment was carried out in order to check whether the proposed family of invariants shows a good behavior for the same task in noisy environments. As explained before, usually images are fed into the system with arbitrary amounts of noise masking the actual information, so this experiment will reflect what the actual behavior of the descriptor set would be in a real application. For this sake, the retrieval experiment on binary images has been repeated twice, one for the same 100 images corrupted with additive Gaussian noise up to a $SNR_{in} = 1$, and another with a Gaussian noise yielding a $SNR_{in} = 0.5$. Results are shown in Fig. 5.

As shown in Fig. 5 results are once again very similar, confirming that the proposed family of invariants have got the same overall behavior as Zernike moments, even in noisy environments. These results are summarized in Table 2, where numerical values of precision for different key sizes of the retrieval set are shown.

5. Conclusions

In this paper, a set of invariants has been introduced, having the same properties and description power as Zernike moments but requiring much shorter descriptions to achieve these results. These new invariants have been derived from the concepts of Hilbert space and Hilbert basis, and share with Zernike invariants the properties of rotation invariance and orthonormality, that yields optimal descriptions of the images to be analyzed.

The new set of moments has been tested against additive Gaussian noise to measure its ability to filter it and preserve image information, showing a behavior that forces to keep shorter descriptions than those based on Zernike moments. This has forced the use of low order moments to analyze an image. Nevertheless, the same results in an image retrieval task can be achieved using a descriptor which is 40% shorter than the Zernike based, not only using clean instances of images for querying, but using instances corrupted with different amounts of additive Gaussian noise as well.

References

Bovik, A., 2009. The Essential Guide to Image Processing. Academic Press.

Chen, G., Xie, W., 2011. Wavelet-based moment invariants for pattern recognition. Optical Engineering 50 (7), 077205-1–077205-9.

Fei-Fei, L., Fergus, R., Perona, P., 2004. Learning generative visual models from few training examples: an incremental Bayesian approach tested on 101 object categories. In: IEEE CVPR Workshop on Generative-Model Based Vision.

Flusser, J., 2000. On the independence of rotation moment invariants. Pattern Recognition 33, 1405–1410.

Flusser, J., Suk, T., Zitova, B., 2009. Moments and Moment Invariants in Pattern Recognition. John Wiley and Sons Ltd.

Hewitt, E., Hewitt, R.E., 1979. The Gibbs–Wilbraham phenomenon: an episode in Fourier analysis. Archive for History of Exact Sciences 21, 129–160.

Hu, M.-K., 1962. Visual pattern recognition by moment invariants. IRE Transactions on Information Theory 8, 179–187.

Khotanzad, A., Hong, Y.H., 1990. Invariant image recognition by Zernike moments. IEEE Transactions on Pattern Analysis and Machine Intelligence 12 (5), 489–497.

Lee, B.Y., Tarng, Y.S., 1999. Application of the discrete wavelet transform to the monitoring of tool failure in end milling using the spindle motor current. International Journal of Advanced Manufacturing Technology 15, 238–243.

Mukundan, R., 2004. Some computational aspects of discrete orthonormal moments. IEEE Transactions on Image Processing 13 (8), 1055–1059.

Rao, G.P., 1983. Piecewise Constant Orthogonal Functions and Their Application to Systems and Control. Spinger Verlag.

Reiss, T.H., 1991. The revised fundamental theorem of moment invariants. IEEE Transactions on Pattern Analysis and Machine Intelligence 13 (8), 830–834.

Rudin, W., 1991. Functional Analysis. McGraw Hill.

Teague, M.R., 1980. Image analysis via the general theory of moments. Journal of the Optical Society of America 70 (8), 920–930.

Teh, C.-H., Chin, R.T., 1988. On image analysis by the methods of moments. IEEE Transactions on Pattern Analysis and Machine Intelligence 10 (4), 496–512.

Xu, D., Li, H., 2008. Geometric moment invariants. Pattern Recognition 41, 240–249.